On the nature of radar backscatter and 250 MHz scintillation linked with an intense daytime E_s patch

A. K. Patra,[1] P. Pavan Chaitanya,[2] and A. Bhattacharyya[3]

Received 5 July 2011; revised 28 December 2011; accepted 12 January 2012; published 10 March 2012.

[1] In this paper we present and analyze the Gadanki radar observations of an unusual event of daytime radar echoes from the *E* region, which spread over a range of 105–150 km and displayed a "U shape" in the range-time SNR map. The U shape echoing structure was an added feature to the commonly observed lower *E* region echoes with slowly descending features and 150 km echoes with range migration displaying a forenoon descent and afternoon ascent. Distinctly different Doppler velocities were observed in the two arms of the U shape structure with velocities increasing with height and surprisingly exceeding the Doppler velocities of the 150 km echoes. The Doppler spectra display features very similar to those observed below 100 km indicating turbulence as the underlying process. A collocated ionosonde observed unusually strong sporadic *E* (E_s) activity with maximum reflected/scattered frequency (f_tE_s) reaching 16 MHz in close correspondence with the U shape structure. During the same duration, a collocated 250.6 MHz scintillation receiver revealed scintillation activity, not observed before from Gadanki. The unusual radar observations, strong E_s activity, and daytime scintillation are first of its kind from Gadanki. Detailed analysis suggests that the U shape radar echoes extending to 150 km range were due to the sidelobe detection of the *E* region irregularities with special features that were also responsible for the daytime scintillation. The genesis and implication of the irregularities are discussed.

Citation: Patra, A. K., P. P. Chaitanya, and A. Bhattacharyya (2012), On the nature of radar backscatter and 250 MHz scintillation linked with an intense daytime E_s patch, *J. Geophys. Res.*, *117*, A03315, doi:10.1029/2011JA016981.

1. Introduction

[2] Much of the understanding on the off-electrojet low-latitude *E* region plasma irregularities has come though the radar observations of field-aligned irregularities (FAI) made in the last one decade from Gadanki (6.5°N dip latitude) in India, Piura (7°N dip latitude) in Peru, and Kototabang (11.4°S dip latitude) in Indonesia [e.g., *Chau et al.*, 2002; *Patra et al.*, 2004, 2007, and the references therein]. Based on the basic features of the FAI observations, the gradient drift instability and related turbulence were invoked as the governing processes. The descending properties of the echoing regions and quasiperiodic echo occurrence provided important direction in identifying the role of tidal and gravity wave associated wind shear in the low-latitude plasma irregularity process [*Patra et al.*, 2004; *Choudhary et al.*, 2005; *Venkateswara Rao et al.*, 2008]. One attempt was also made to unravel the linkage between radar echoes and the E_s activity [*Patra et al.*, 2005a]. Although the roles of neutral wind and E_s were invoked, roles of the neutral wind in the gradient drift instability process have been detailed only recently [*Patra et al.*, 2009; *Li et al.*, 2011].

[3] While most of the low-latitude *E* region FAI observations were found to be consistent with those expected from the gradient drift instability process, the observations reported by *Yokoyama et al.* [2009], based on the Equatorial Atmosphere Radar observations, could not be accounted for. They observed the daytime echoes coming from altitudes as high as 120 km, where echoes observed in the east beam were stronger than those in the west, an asymmetry that was different from those observed in the *E* region echoes below 100 km and also the 150 km echoes. Intriguingly, these echoes displayed type-2 Doppler spectra, which are characterized by low mean Doppler velocities (much smaller than ion acoustic speed) and fairly broad spectral width and indicate a turbulent process as their origin. On the other hand, from electrojet studies, we know that irregularities formed during the daytime around the peak altitude of hall conductivity, which is around 105 km, due to the electrojet flow are interpreted in terms of a modified two-stream instability, which requires electron drift to exceed the ion acoustic speed, and manifest type-1 Doppler spectrum. Type-1 spectra have mean Doppler velocities close to the ion acoustic speed (360 m s^{-1}) and spectral widths much narrower than their mean Doppler velocities. Thus the echoes,

[1]National Atmospheric Research Laboratory, Gadanki, India.
[2]Department of Physics, Sri Venkateswara University, Tirupati, India.
[3]Indian Institute of Geomagnetism, Navi Mumbai, India.

0148-0227/12/2011JA016981

Table 1. Specifications Used for the Radar Observations

Parameter	Value
Inter-pulse Period (IPP)	1.3 ms
Pulse width	8 μs
Number of coherent integrations	16
Number of FFT points	128
Number of incoherent integrations	10
Range coverage	69–187.8 km
Range resolution	1.2 km
Time resolution	55 s
Nyquist velocity limit	$\pm$68 m s^{-1}
Velocity resolution	1.06 m s^{-1}

displaying type-2 spectra, from the upper *E* region observed by *Yokoyama et al.* [2009] continue to be elusive.

[4] In this paper we present and analyze simultaneous observations of VHF radar echoes from the daytime *E* region extending to unusually high altitude, scintillation of satellite signal at 250.6 MHz, and complex E_s structures, all made from Gadanki. The daytime scintillation observations are the first of their kind from Gadanki. An investigation on the low-latitude *E* region plasma irregularities of this kind using three different radio diagnostics has not been performed before. We also attempt to provide physical insight on the intriguing upper *E* region echoes reported earlier by *Yokoyama et al.* [2009].

2. Experiment Description

[5] Radar observations of FAI, which motivated the present study, were made on 29 August 2009. Geomagnetic condition was quiet, as characterized by A_p = 2. Radar observations were made using the 53 MHz MST radar located at Gadanki [*Rao et al.*, 1995]. Radar parameters used in the experiment are given in Table 1. It should be mentioned that in the present observations, 8 linear subarrays, each consisting of 32 antennas, on the northernmost part of the antenna array was not functional due to technical problems. In addition, some of the coupler used in the feeder system were not working resulting in significant deterioration in the antenna pattern. The North-South beam width (half power full width) was estimated to be 3.7° instead of 2.8°. The East-West beam width, however, was 2.8°. More details on the antenna configuration and feeder network can be found elsewhere [*Rao et al.*, 1995]. We positioned the antenna beam at an angle of 14° off-zenith due magnetic north, which satisfies perpendicularity to Earth's magnetic field in the height region of 90–180 km due to the finite antenna pattern. Such experiments are being made at Gadanki on a few days every month to study the *E* and

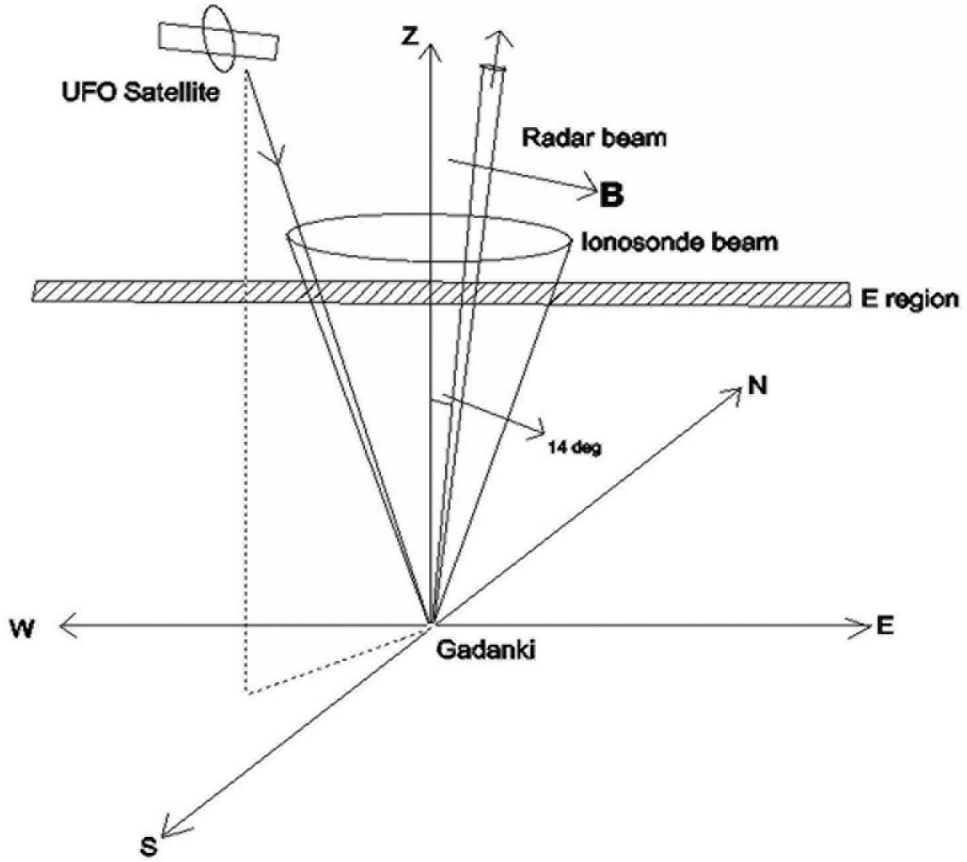

Figure 1. Schematic showing the antenna beam configuration of the Gadanki radar, ionosonde field of view, and line-of-sight path for the VHF scintillation receiver. More details on this configuration are given in section 2.

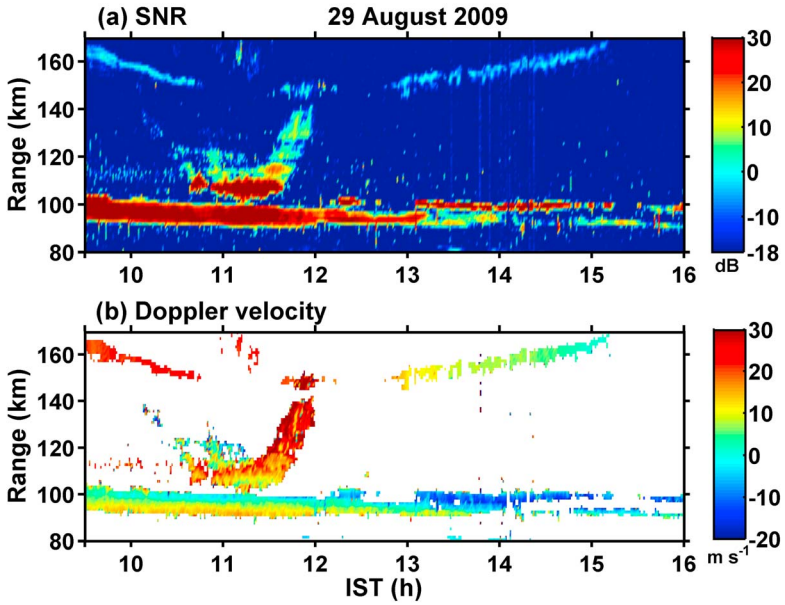

Figure 2. Range-time variations of (a) SNR and (b) Doppler velocity of the radar echoes observed from the *E* and 150 km regions on 29 August 2009.

150 km region FAI simultaneously. Since the 150 km echoes are weak and their mean Doppler velocity and spectral width are <30 m s^{-1} and <15 m s^{-1}, respectively, we performed coherent integration of 16 pulse returns leading to a observational Doppler window of ±68 m s^{-1}. Except for very strong turbulent activity, this observational Doppler window proves to be adequate for the daytime *E* region FAI observations from Gadanki. In the present observations, we found that on a few occasions the spectral energy has extended to the edges of the Doppler window but did not cause any serious limitation to the present investigation.

[6] Observations of E_s were made every 15 min using a collocated digital ionosonde (IPS-42). This ionosonde works in the frequency range of 1–22.6 MHz and uses delta antennas for transmission and reception. The antenna beam width (half power full width) varies with frequency and lies in the range of 30–60° in the frequency range of 1–15 MHz (60° at 6 MHz and lower beam width for lower as well as higher frequencies). Received signals are recorded in the form of ionogram with a range resolution of 3 km.

[7] Scintillation observations correspond to satellite signal at 250.6 MHz from a geostationary satellite, UFO-2 located at 71.2° E. The azimuth (with respect to geographic north) and zenith angles of the satellite with respect to Gadanki are 214° and 29°, respectively. Satellite signals were sampled at the rate of 20 Hz. It may be mentioned that due to a technical snag, data acquisition could be made continuously for ∼12 min at a time and we could capture two such data sets during a scintillation event that took place between 1102 IST and 1140 IST on 29 August 2009.

[8] In order to show the overlap of the ionospheric regions seen by the three radio diagnostics (radar, ionosonde and VHF scintillation) a schematic, illustrating the look angle of the Gadanki radar beam, ionosonde field-of-view, and the satellite-to-ground receiver link, is shown in Figure 1. Note that while the radar and the ionosonde probed some common volume of the *E* region, the penetration point at the *E* region (at ∼105 km) for the 250.6 MHz signal path to Gadanki, which was (13.1° N, 78.9° E), was located toward West-South of the volume probed by the radar/ionosonde.

3. Observational Results

3.1. Radar Observations

[9] Figures 2a and 2b present range-time variations of SNR and Doppler velocity, respectively, of the echoes observed on 29 August 2009. Doppler velocities represent FAI drifts transverse to Earth's magnetic field in the North-South plane. Positive (negative) velocity represents FAI drifts upward northward (downward southward). From Figure 1a, one can notice three echoing regions: (1) a slowly descending echoing region below 100 km altitude, which is commonplace in the Gadanki radar observations [*Patra et al.*, 2004], (2) the 150 km echoing layer displaying classical forenoon descent and afternoon ascent, which is observed quite frequently at Gadanki [*Patra and Rao*, 2007], and (3) echoes occurring during a brief period of 1000–1200 IST in between the usual *E* region echoes (item 1) and the 150 km echoes (item 2), hereafter called "intermediate-region." In the following we will focus on the echoes associated with the intermediate-region and bring in the other echoes (items 1 and 2) for comparative study wherever necessary.

[10] As far as the intermediate-region echoes are concerned, they are unusual since they occurred at altitudes higher than those observed commonly during daytime. More importantly these echoes display remarkable altitude structures, resembling a U shape, where the echoes in the left-wing have lower SNR than those in the right wing. The echoes in the bottom part of the U shape, which are centered on 107 km, have SNR as high as 36 dB, while those on both the wings of the U shape are 20–40 dB lower than

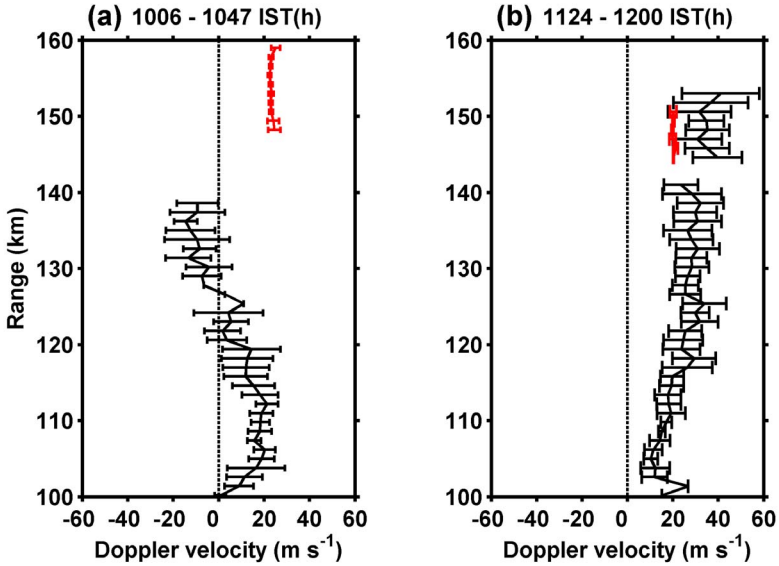

Figure 3. (a) Mean and standard deviation of Doppler velocities associated with the left wing of intermediate region echoes (in black color) and Doppler velocities of 150 km echoes (in red color) observed during 1006–1047 IST. (b) Same as Figure 3a, but for right wing of the intermediate-region echoes (in black color) observed during 1124–1200 IST and for 150 km echoes (red color) observed during 1132–1147 IST.

those of the bottom part. The bottom part of the U shape echoing pattern, consisting of two patches with a very brief break during 1049–1052 IST, was observed during 1037–1140 IST. Further, while the echoes display a U shape structure, through close examination we find that the U shape is composed of a number of clumps spread over a wide range starting from 105 km to 150 km. For the right arm of the U shape, we could clearly find four clumps centered on 115 km, 121 km, 130 km and 150 km ranges having echo SNR as high as 16 dB, 8 dB, 6 dB, and −4 dB, respectively. It should be mentioned that SNRs of the topmost clump centered at ∼150 km range are such that it is difficult to distinguish these from the well known 150 km echoes if the Doppler velocities and spectral width associated with these echoes are not examined.

[11] The Doppler velocities of the 150 km echoes are positive, indicating upward northward velocity, and hence represent eastward electric field. As far as the velocities in the intermediate-region echoes are concerned, they are mostly positive, except for some associated with the left-wing echoes, which are negative. It can also be noted that in general the Doppler velocities in the right-wing echoes are more than those of the left-wing echoes. It is important to note that the velocities in the topmost clump (at 150 km range) are remarkably larger than those of the well-known 150 km echoes. The velocities observed in the bottommost echoing region (<100 km), however, are different from those observed above 100 km and they are presumed to be due to the combined effect of the zonal electric field and neutral wind (meridional and/or vertical) owing to collisional coupling of the plasma with the neutrals at that height [*Krishna Murthy et al.*, 1998].

[12] Another important aspect of the intermediate-region echoes is the height variation of the Doppler velocities. In order to show this feature clearly, we present the mean and standard deviation of Doppler velocities observed during 1006–1047 IST (corresponding to the left wing) and 1124–1200 IST (corresponding to the right wing) in Figures 3a and 3b, respectively. In Figure 3b the Doppler velocity of the 150 km echoes corresponds to the measurements made during 1132–1147 IST. This has been done in order to distinguish the 150 km echoes from those observed for the topmost clump of the U shape, which also appeared at the same range. For the left wing, the Doppler velocities, which were in the range of −15–20 m s^{-1}, changed from positive at lower range to negative at higher range with a crossover range of 125 km. Note that the Doppler velocities of the 150 km echoes are ∼22 m s^{-1} and show no height variation, a feature consistent with the earlier report [*Patra and Rao*, 2006]. For the right wing, however, the Doppler velocities, which were in the range of 15–36 m s^{-1}, increased with range. It is important to mention that the range rate (dr/dt) of the echoes observed in the second and third clumps are estimated to be 20 m s^{-1}, which agree well with the observed Doppler velocities. It is interestingly to note that the velocities for the 150 km range associated with the topmost clump of the U shape was 36 m s^{-1} as against 18 m s^{-1} for the 150 km echoes. In this case also, the Doppler velocities of the 150 km echoes show no height variation, but the velocities are lower than those observed during 1106–1047 IST. The observed lower velocities during 1132–1147 IST than those during 1006–1047 IST are consistent with those reported earlier, which showed a decrease in velocity with local time [*Patra and Rao*, 2007]. Later, we will make a detailed analysis on the left wing and right wing velocity asymmetry and also the height variation of velocity.

[13] To gain further insight, we present the spectral features of the echoes in Figures 4a and 4b. Figure 4a shows Doppler power spectrum as a function of range observed at 1132:57 IST. It is important to note that the spectra observed

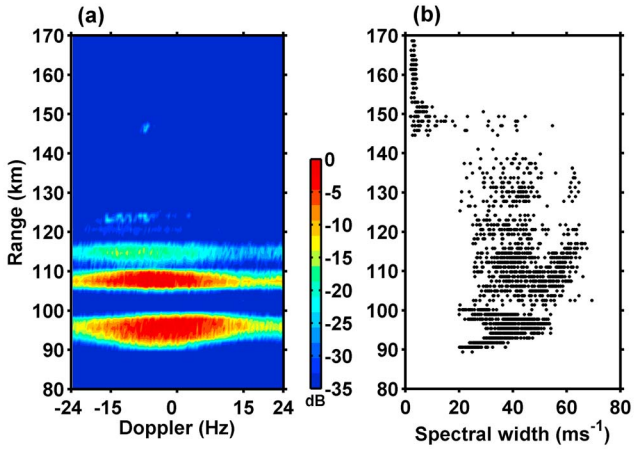

Figure 4. (a) Doppler power spectrum observed at 1132:57 IST and (b) spectral width (2σ) of the echoes observed during 1000–1200 IST in the form of scatterplot.

in the 100–120 km range were very similar to those observed below 100 km. Another echoing region located at ~122 km, which started appearing at that time, also showed broad spectral features. Later, when the echo strength developed and two echoing layers were observed in the 120–135 km range, spectral features were found to be very similar to those observed below 120 km. In contrast, the echoes observed at 145 km were narrow and they were the well-known 150 km echoes. In order to illustrate the spectral broadening at different heights quantitatively, we present spectral width (2σ) of the echoes observed during 1000–1200 IST in the form of scatterplot in Figure 4b. It is very clear from Figure 4b that the spectral width observed in the 100–145 km range are as high as 65 m s^{-1}, which are larger than those observed as 55 m s^{-1} below 100 km. Another striking aspect is that some echoes observed in the 140–145 km range are as high as 50 m s^{-1}, which is much larger than those of the classical 150 km echoes (2–10 m s^{-1}) [*Patra and Rao*, 2006]. This clearly suggests that echoes with large spectral width observed at ~150 km range are not of 150 km altitude origin.

3.2. E_s Observations

[14] E_s characteristics are illustrated in Figures 5 and 6. Figure 5a shows f_tE_s (maximum frequency reflected/ scattered) values observed during 27–31 August 2009, which clearly show that E_s activity was strikingly high during 1045–1200 IST on 29 August, with a maximum f_tE_s of 16 MHz. As mentioned earlier, we also observed height structures in the E_s layer on 29 August. In order to illustrate the height-time variation of E_s activities, f_tE_s and $h'E_s$ (virtual height of E_s) are shown in Figures 5b and 5c, respectively. Note that while only one layer was observed during 1045–1145 IST and $h'E_s$ was ~112 km, during 1200–1300 IST, E_s occurred at two distinctly different heights—the upper one being at ~117 km and the lower one being at ~105 km. Also note that at 1200 IST, f_tE_s values were very different (5 and 12 MHz). The descending trend in $h'E_s$ agrees well with that of the bottommost radar echoing layer, which is similar to that reported earlier by *Patra et al.* [2009].

[15] In order to illustrate the type of E_s, we show, in Figures 6a–6d, a few ionograms taken at 1030 IST, 1115 IST, 1200 IST, and 1400 IST, respectively. Although the ionograms include both ordinary and extraordinary modes, it is difficult to distinguish them since the E_s echoes are overwhelming and the F region echoes are either weak or not seen due to strong E_s activity. Figure 6a shows an ionogram taken at 1030 IST when a strong radar echoing layer with a thickness of ~7 km confining to altitudes below 100 km was observed. The ionogram, shown in Figure 6b, which was taken at 1115 IST, shows strong E_s activity with f_tE_s as high as 16 MHz. Also note that F layer trace was not observed, indicating that the E_s was blanketing type. It is interesting to note that during this time an additional strong echoing layer centering on 107 km was observed by the radar. Figure 6c shows an ionogram taken at 1200 IST when the additional echoing layer was absent. At this time, however, two distinctly different echoing layers were observed by the ionosonde. It may be recalled that while the radar observations at 1200 IST show one echoing layer quite similar to that observed at 1030 IST, the radar echoes observed at 1220 IST show two well separated echoing layers. The detection of two echoing layers in the ionogram at an earlier time (at 1200 IST) than that of radar observations (at 1220 IST) seems to suggest that the upper echoing layer was from a laterally different physical location and the early detection of these echoes was possible due to the large beam width of the ionosonde system. Subsequently, when the echoing region drifted through the radar beam, they were detected by the radar. Figure 6d shows an ionogram taken at 1400 IST, which shows E_s with second reflection, is found

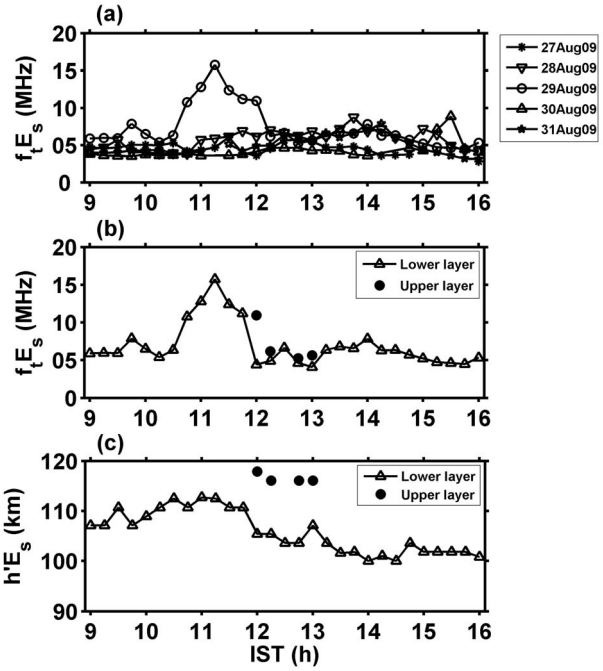

Figure 5. (a) f_tE_s (maximum frequency reflected/scattered) values observed during 27–31 August 2009. Detailed variations of (b) f_tE_s and (c) $h'E_s$ (virtual height of E_s) observed on 29 August 2009.

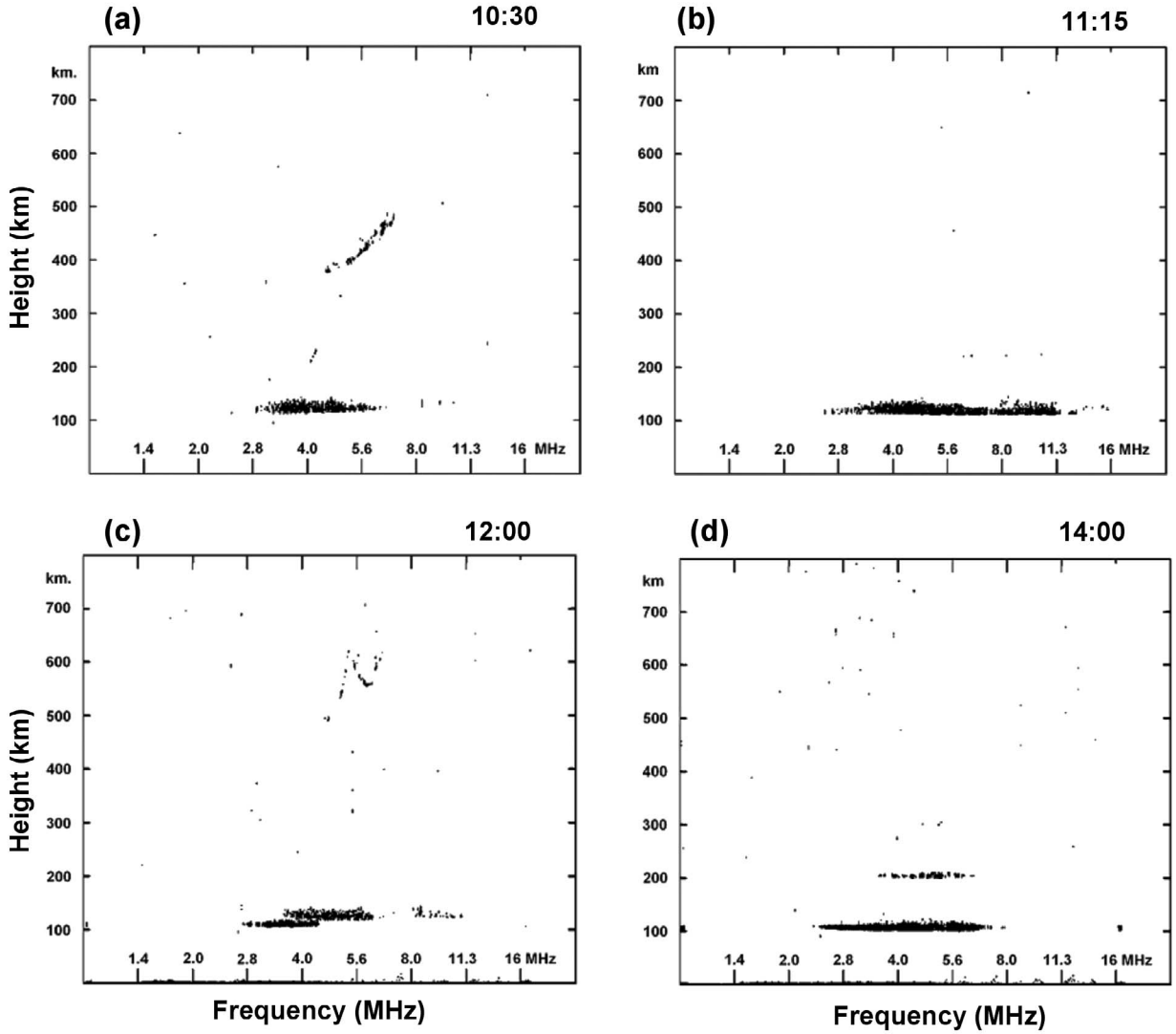

Figure 6. Ionograms observed at (a) 1030 IST, (b) 1115 IST, (c) 1200 IST, and (d) 1400 IST, which correspond to different features of the radar echoes. Ionograms include both ordinary and extraordinary modes. For details, refer to the text.

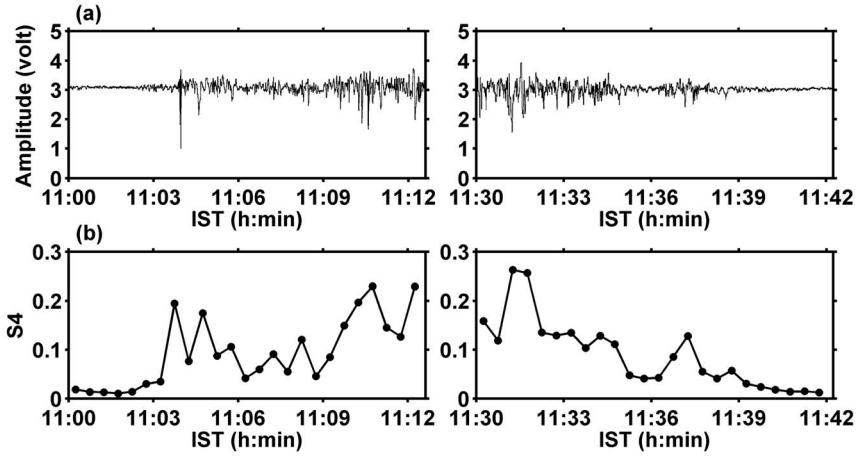

Figure 7. (a) Scintillation observations made during (left) 1100–1113 IST and (right) 1130–1142 IST. (b) Corresponding scintillation index, S_4 (calculated using 30 s of data).

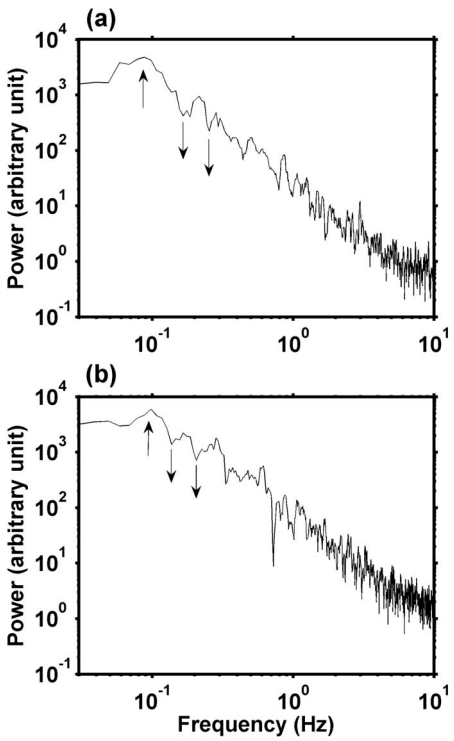

Figure 8. Power spectra on log-log scale corresponding to the scintillation observations of (a) 1104:40–1106:36 IST and (b) 1131:44–1133:22 IST. Upward (downward) arrows indicate the Fresnel frequency (Fresnel minima).

to be blanketing type with f_tEs of 8 MHz. During this time, however, the radar echoes were seen in the form of two thin and distinctly different echoing layers.

3.3. Scintillation Observations

[16] Figure 7a shows scintillation observations made during 1100–1113 IST (left panel) and 1130–1142 IST (right panel). Corresponding scintillation index, S_4 (calculated using 30 s of data) are shown in Figure 7b. Maximum S_4 value is 0.27, which is similar to those reported for the daytime scintillation for the dip equatorial/ low-latitude *E* region irregularities observed at 140 MHz [e.g., *Bhattacharyya and Rastogi*, 1986]. As is evident, scintillation started at ~1102 IST and ended at ~1140 IST. Also, scintillation was patchy in nature indicating the patchy nature of the irregularities. Notably, the present observations are closely linked with intense E_s activity observed overhead and are very similar to those reported earlier by *Rastogi et al.* [1977] based on observations made from near equatorial locations.

[17] Figures 8a and 8b show the power spectra on log-log scale corresponding to the two data sets. The slopes of the high frequency asymptotes are estimated to be about −3. For weak scintillations, as is the case here, this spectral slope is an estimate of a two-dimensional power law spectrum of the irregularities that produce the scintillations. *Bhattacharyya and Rastogi* [1986] also obtained a spectral slope of around −3 in their study of the daytime amplitude scintillations observed near the dip equator on multifrequency signals. This estimate of the two-dimensional irregularity spectral index is close to the value of −8/3 obtained by *Sudan* [1983] for the inertial range irregularities associated with the equatorial electrojet irregularities. Further, according to weak scintillation theory and for thin irregularity layer, which is applicable to the *E* region irregularities, the power spectrum of amplitude scintillations is expected to display Fresnel oscillation owing to the oscillatory nature of the Fresnel filter function [e.g., *Rufenach*, 1972]. In the present case, we could notice a clear signature of the Fresnel frequency as well as the minima. In the first data set, the Fresnel frequency is 0.08 Hz and the first and second minima are 0.165 Hz and 0.253 Hz, respectively. In the second data set, the Fresnel frequency is 0.09 Hz and the first and second minima are 0.136 Hz and 0.2 Hz, respectively. Later, we will use these to estimate the horizontal drifts of the irregularities and compare the estimated horizontal drifts with those of the radar observations.

4. Discussion

[18] The important observations linked with the intermediate-region can be summarized as follows.

1. Radar echoes from unusually large range, referred to as intermediate-region, displayed a U shape structure with asymmetric echo power and Doppler velocity.
2. Spectral characteristics of the intermediate-region echoes were similar to those of the *E* region echoes observed below 100 km altitude and very much dissimilar to those of the 150 km echoes.
3. Doppler velocities of the intermediate-region echoes showed increasing trend with height and surprisingly exceeded those of the 150 km echoes.
4. Unusually strong E_s with maximum f_tE_s of 16 MHz was observed coinciding with the period of the radar observations of the bottom part of the U shape echoes.
5. Intense echoes in the right wing of the U shape and the splitting of the E_s layer at the end of the event were observed simultaneously.
6. Scintillation was observed during the period of the unusual E_s event and unusual radar echoes and displayed patchy nature of the irregularities.

[19] We also noted that the 150 km echoes disappeared during 1045–1135 IST and 1215–1250 IST. The period of first disappearance of these echoes coincides with that of the U shaped echoing event. The disappearance of these echoes during 1215–1250 IST, however, occurred when there was no U shaped echo event. These suggest that the disappearance of the 150 km echoes is not related to the U shaped echo event. Instead, these indicate that the 3 m irregularities, responsible for the 150 km echoes, were so week during those periods that they could not be detected by the radar.

[20] At the first look, the characteristics of intermediate-region echoes, in terms of the U shape, Doppler velocity, and spectral width, appears quite mysterious. Especially, the altitude of their occurrence during the day is unusually high and there exists no known physical mechanism that could simply account for such echoes. On the other hand, the spectral characteristics indicate the involvement of a turbulent process akin to that of the lower *E* region. Also the Doppler velocities of the intermediate-region echoes exceeded those of the 150 km echoes, which could not be accounted for by the zonal electric field effect alone. If the

echoes were received by the main beam, which was pointed at 14° off-zenith due north to make it perpendicular to Earth's magnetic field, the line-of-sight Doppler velocities of the U shaped echoes are expected to be mainly governed by the zonal electric field since the contribution of neutral wind along the line-of-sight would be very small due to the very low value of ψ ($= \nu_e\nu_i/\Omega_e\Omega_i$) at that height region. This being the case, we expect the Doppler velocities to be close to those of the 150 km echoes. This, however, is not the case and thus we believe that larger Doppler velocity than expected was due to the contribution of zonal plasma drift along the line-of-sight. However, if it had to happen, the line-of-sight, along which the echoes were detected, should have finite azimuth angle. The main beam, however, was in the North-South plane with an off-zenith angle of 14°. This implies that the mysterious echoes might have been received by sidelobes in the azimuthal plane which satisfied perpendicularity to magnetic field, a condition to be satisfied for detecting the field-aligned irregularities. Thus, in all likelihood, the U shaped echoes were linked with irregularities of much lower altitude origin but appeared at higher range due to the sidelobe detection. This guess, however, would invite a counter question—why echoes were detected through the sidelobes only during a brief period while *E* region echoes having similar SNR were detected at other times of the day as well? We address this issue in detail later. We also discuss the roles of gradient drift instability and zonal neutral wind in manifesting these observations.

[21] We have also noted that E_s activity was unusual with maximum f_tE_s being 16 MHz, and associated scintillation. Further, both were observed for short duration coinciding with the radar observations. It may be recalled that the intense E_s patch was observed during 1045–1200 IST and the bottom portion of the U shape echoes was observed during 1037–1140 IST, while scintillation was observed during 1102–1140 IST, which appears to be linked with the second patch of the bottom part of the U shape structure observed during 1055–1140 IST. It is important to note that the *E* region of the ionosphere probed by the scintillation receiver from Gadanki was west of those observed by the radar/ionosonde and the scintillation was observed with a delay with respect to those observed by the radar/ionosonde. These suggest that the zonal drift of the irregularity patch was westward. More detailed analysis on the zonal drift based on the radar and scintillation observations is made and discussed in section 4.2. As far as the echoes in the right wing of the U shape echo structure with large range extent are concerned, it is striking to note the splitting of the E_s layer at the end of the event and also the patchy nature of scintillation. It is quite likely that the splitting of E_s layer and associated upper layer are related to the detection of oblique echoes from patchy E_s.

4.1. On the Sidelobe Detection

[22] Two intriguing aspects of the U shape echoes which have possible connectivity to the sidelobe detection in question are: (1) large spectral width observed at all altitudes up to 150 km, and (2) asymmetry in the velocities of the left and right wings of the U shape echoes. In the following we discuss the sidelobe perspective in detail.

[23] As far as the daytime 150 km echoes are concerned, which occur between 140 and 170 km altitudes at Gadanki, their spectral widths are well below 15 m s^{-1} [*Patra and Rao*, 2006, 2007]. Similar spectral width has been found for the 150 km echoes observed in the present observations also. For a brief period around 1145 IST and for the height region of 140–145 km, the spectral width values, however, were much larger than those of the 150 km echoes. We surmise that the echoes having spectral width as high as 50 m s^{-1} observed from 150 km range, in all likelihood, are of lower altitude origin, where plasma turbulence is strong and it is very likely that these echoes were detected by the sidelobes.

[24] The other observation which strongly supports the sidelobe detection perspective is the Doppler velocities of the echoes. For the echoes in the 120–140 km range, we find that the Doppler velocities in the right wing of the U shape echo structure are remarkably larger than those of the left wing. Considering that the *E* region FAI at 110 km have upward northward motion, which is due to the daytime eastward electric field (which is consistent with the upward northward motion of the 150 km echoes), the velocity difference observed in the two wings of the U shape can be visualized as due to the zonal motion and such a scenario could occur if the echoes are observed with beams looking east/west of the magnetic north. Since the main beam was looking transverse to magnetic field in the magnetic North-South plane, it is only possible if the echoes are detected by the sidelobes looking toward east/west.

[25] For the westward moving ionospheric *E* region plasma and for the frozen-in plasma structures, the irregularity structures in the SNR map (Figure 2) from left to right can be viewed as west-to-east plasma structures. In the case of westward moving *E* region plasma and for the sidelobe detection of the radar echoes, it is expected that the eastward (westward) looking sidelobe would detect the irregularities first (last). Accordingly, the irregularities would be detected by the main beam once they passed by the eastward looking sidelobe. The fact that the left-wing (right-wing) echoes were observed earlier (later) than the bottom echoes of the U shape supports this notion very well. This will be further clarified from the velocity and spectral width observations.

[26] For the westward and upward northward motion of the plasma irregularities (which is the usual daytime scenario), we can write the radial velocities observed by conjugate East-West beam pair as:

$$V_{rE} = -V_z \,\mathrm{Sin}\alpha + V_{\perp_B} \,\mathrm{Cos}\alpha, \tag{1}$$

$$V_{rW} = V_z \,\mathrm{Sin}\alpha + V_{\perp_B} \,\mathrm{Cos}\alpha, \tag{2}$$

where, V_{rE} and V_{rW} are the radial velocities observed by the east beam and the west beam, V_z is the zonal velocity (westward positive), $V_{\perp_B}$ is the velocity along north-14° (upward northward positive), and α is the look angle of the east/west sidelobes with respect to north-14°. From the above equations, it is clearly evident that for irregularities moving westward and upward northward, large positive velocities observed in the right wing of the U shape echo structure should be associated with the westward looking sidelobe signals and similarly the less positive or negative velocities observed in the left wing should be associated with those of the eastward looking sidelobe. Moreover it is also expected that the westward moving plasma structures

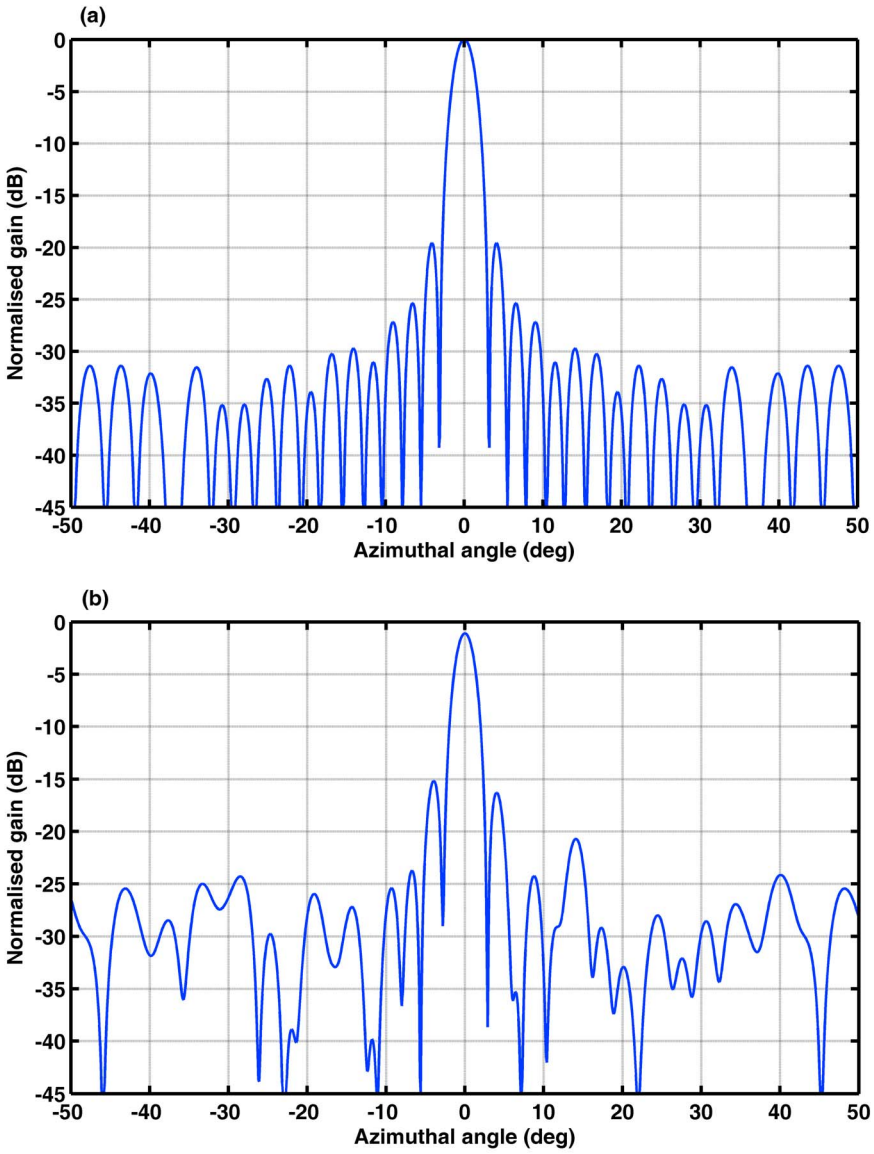

Figure 9. Antenna pattern corresponding to (a) the idle situation involving the whole array consisting of 1024 Yagi antennas and (b) the reduced number of antenna elements due to malfunctioning during the present observations. These represent the azimuthal pattern when the antenna array is phased to tilt the main beam at 14° off zenith toward north, which satisfies perpendicularity to Earth's magnetic field.

would appear earlier in the eastward looking sidelobe than in the westward looking sidelobe. Thus the velocity asymmetry and large spectral width with poor SNR associated with the U shape echo structure clearly suggest that that the echoes are due to sidelobe detection.

[27] Having argued that the intermediate region echoes are due to the sidelobe detection, it is also important to note that such sidelobe detection has not been possible at other times. This implies that the sidelobe detection just mentioned is not simply applicable to every *E* region echo having comparable SNR. In fact the bottommost irregularities (below ~100 km), which gave rise of radar echoes with similar SNR, were not detected by the sidelobe. This implies that the irregularities associated with the bottom part of the U shape echoes must be of special type.

[28] Considering that the bottommost echoing region in the U shape pattern is due to the main lobe and the four clumps in the right wing of the U shape pattern are due to sidelobe detection, the echo ranges of the four clumps observed through the sidelobes can be used to estimate the sidelobe look angles, α as:

$$\alpha = \mathrm{Cos}^{-1}(\mathrm{r}/\mathrm{r}_{\mathrm{sl}}), \tag{3}$$

where r is the range of the bottommost echoing layer, which is 107 km, and r_{sl} is the range of the sidelobe echo. For the right-wing echoes, the look angles of the sidelobes (i.e., α) are estimated to be 21°, 28°, 34°, and 44° corresponding to the four discrete echo ranges of 115 km, 121 km, 130 km and 150 km, respectively. It may be important to mention

that although the first three side lobes of the antenna pattern are stronger than those close to these angles, the look angles of the first three side lobes are less than 9°. This implies that if the echoes were detected by the first three side lobes, the echo range for the third side lobe (the farthest one among the first three side lobes) would be 108.3 km, which is higher by one range gate (1.2 km) only. The observed echo ranges of the four clumps, however, are much higher than 108.3 km, suggesting that the side lobes in questions are not the first three side lobes but are those in the angular range of 21°–44°.

[29] In an effort to account for the U shape echoes in terms of side lobe detection, we present two antenna patterns, one for the condition when all antennas work properly and another for the condition applicable to the present observations, in Figures 9a and 9b, respectively. These represent the azimuthal antenna pattern containing the main beam tilted at 14° off zenith toward north, which satisfies perpendicularity to the Earth's magnetic field. Since the Gadanki radar antenna array is aligned along the geomagnetic axis, and the declination angle is ~1°, all the side lobes in the azimuthal plane essentially lie in a plane perpendicular to Earth's magnetic field and hence would satisfy the condition for detecting the echoes from the FAI. Note from Figure 9a that the side lobes in between 20° and 44°, which are of interest here, are ~32 dB lower than the main lobe. The antenna pattern corresponding to the present observations, shown in Figure 9b, however, was distorted significantly. Note that the side lobes at azimuth angles of 19.1°, 28°, 33.8°, and 43.5° on the negative *x* axis (representing westward looking side lobes), which are close to those estimated for the side lobe detected echoes as 21°, 28°, 34°, and 44°, are −26 dB, −24.2 dB, −25 dB, and −25.5 dB, respectively, lower than the main lobe. Also note that the side lobe levels on the positive *x* axis (representing eastward looking side lobes) are not similar to those in the negative *x* axis. It should be mentioned that the antenna pattern is computed based on the information available in the system maintenance log book corresponding to a maintenance period much before the present observations and the deterioration in the azimuthal side lobe level was mainly due to the malfunctioning of the coupler in the feeder network along the linear subarrays. The true situation could be even worse than this and hence in the side lobe level also.

[30] For the side lobe levels shown in Figure 9b, we expect the SNR associated with the side lobe detected echoes to be −52 dB, −48.4 dB, −50 dB, and −51 dB lower than that of the main lobe. Since the observed maximum SNR is 36 dB, we would expect the side lobe detected echo SNR to be −16 dB, −12.4 dB, −14 dB, and −15 dB. The observed SNR, however, are 16 dB, 8 dB, 6 dB, and −4 dB, which are 32 dB, 20.4 dB, 20 dB, and 11 dB stronger than those expected. As is evident, the discrepancy for the first clump (centering on 115 km) detected by the azimuthal side lobe of 21° is significant. It is quite likely that the true side lobe level was much worse than that used for the present comparison (i.e., side lobe level was much greater than −26 dB). On the other hand, the echoes in the left wing are much weaker than those of the right wing, indicating that the asymmetric echo strength in the two wings are due the different directional gains of the side lobes looking toward east and west (westward looking side lobes are stronger than those of eastward looking side lobes).

[31] There are three potential sources to account for this discrepancy. It is quite likely that the density fluctuations responsible for the radar backscatter were stronger in the azimuthal directions than those in the north-14°. Such a scenario is similar to that observed as East-West power asymmetry of the electrojet echoes, where the west beam echo power has been found to be higher than those observed in the east beam [e.g., *Patra et al.*, 2005b, and the references therein]. Thus the present observations, which have been linked to the westward looking side lobes, are consistent with those of the electrojet observations. The second source of the discrepancy could be possibly linked with worse antenna side lobe than that shown in Figure 9b. The third likely source could be due to the limiter circuit, which might have clipped the main lobe signals, before feeding to the analog to digital converter. It should be mentioned here that although we have observed a few daytime scintillation events at Gadanki, they are not as strong as the present case. Thus it is quite likely that the main lobe signal was unexpectedly strong and crossed the design limit of the receiver and signal processing system, which was primarily designed for detecting the much weaker echoes from the mesosphere, stratosphere, and troposphere than those of the ionospheric FAI.

4.2. Estimation of Horizontal Drift of the Irregularities

4.2.1. Zonal Drift Estimated Using the Radar Observations

[32] The look angles of the sidelobes (i.e., α) corresponding to the four echoing clumps in the right wing of the U shape, centering on the echo ranges of 115 km, 121 km, 130 km and 150 km, respectively, are estimated to be 21°, 28°, 34°, and 44°. The mean Doppler velocities in the bottommost echoing layer of the U shape are ~10 m s^{-1}, which represents $V_{\perp_B}$, and those in the four clumps (in ascending range) as 20 m s^{-1}, 24.6 m s^{-1}, 28.4 m s^{-1}, and 31.8 m s^{-1} (all from Figure 2b). Using these Doppler velocity values and equation (2), zonal drifts, V_z are estimated to be 30 m s^{-1}, 33.6 m s^{-1}, 35.8 m s^{-1}, and 35.8 m s^{-1}, respectively.

4.2.2. Horizontal Drift Estimated Using the Scintillation Observations

[33] Since we are using the Fresnel frequency (or Fresnel minima) for velocity determination, we could only infer the horizontal drift of the ground scintillation pattern along the magnetic East-West direction given the geomagnetic field-aligned nature of the irregularities. In the present case, however, the structures would be somewhat tilted from the horizontal due to the finite dip angle of the magnetic field (which is 14°) over Gadanki. Using the Fresnel frequency, this horizontal drift speed can be estimated as:

$$V = f\ d_F, \tag{4}$$

where, V is the horizontal drift of the irregularities, f is the Fresnel frequency, and d_F is the Fresnel dimension, which is given as:

$$d_F = (2\lambda z)^{1/2}, \tag{5}$$

where λ is the wavelength of the radio frequency (which is 1.2 m corresponding to 250.6 MHz) and z is the line-of-sight

distance between the irregularity patch and the scintillation receiver. Estimation of z can be done using the azimuth and zenith angles of the satellite with respect to Gadanki, which are 214° and 29°, respectively and the altitude of the irregularly patch.

[34] Considering that bottommost echoing region of the U shape structure in the radar observations is closely linked with intense E_s activity and scintillation, the echo height, h can be estimated as:

$$h = \mathrm{r\ Cos\ }\theta, \tag{6}$$

where, r is the echo range and θ, which is 14°, is the beam zenith angle of the antenna main lobe that satisfies perpendicularity to the Earth's magnetic field. The height of the bottom part of the U shape structure is estimated to be 104 km (= Cos14*107 km).

[35] The line-of-sight distance, z between the E region pierce point and the receiver relevant to the present geometry can be written as:

$$z = (R_E + h)\cos\theta_1 - R_E\cos\theta_0, \tag{7}$$

where R_E, the mean radius of the Earth, is 6371 km; h is 104 km; θ_0, the zenith angle of the signal path with respect to Gadanki, is 29°; and θ_1 is the zenith angle of the signal path at the pierce point corresponding to an altitude of 104 km. Expression of θ_1 can be written as:

$$\cos\theta_1 = \left[1 - R_E^2\sin^2\theta/(R_E + h)^2\right]^{1/2}. \tag{8}$$

Using the above expressions and values, z and d_F are estimated to be 119 km and 534 m, respectively.

[36] Using the Fresnel minima, horizontal velocity can be estimated as:

$$V = f_n(\lambda z/n)^{1/2}, \tag{9}$$

where f_n is the frequency corresponding to nth minima and n is equal to 1 or 2 (in the present case). For the first data set, the horizontal drifts of the ground scintillation pattern are estimated to be 43 m s^{-1} from the Fresnel frequency, and 62 m s^{-1} and 67.5 m s^{-1} from the first and the second minima, respectively. For the second data set, the drifts are estimated to be 47 m s^{-1} from the Fresnel frequency, and 51 m s^{-1} and 53 m s^{-1} from the first and the second minima, respectively.

[37] For the signal path with zenith angle θ_0 and azimuth angle φ at the pierce point, and for the finite dip angle, I of geomagnetic field (which is 14°), drift of the scintillation pattern, V can be expressed as:

$$V = V_z - V_{\perp_B}\tan\theta_0\ \sin\varphi/(\tan\theta_0\ \cos\varphi\sin I + \cos I), \tag{10}$$

where, V_z is the zonal drift (eastward positive), $V_{\perp_B}$ is the drift in a direction perpendicular to **B** in the vertical-meridional plane (upward northward positive). For θ_0 = 29°, φ = 214° and I = 14°, and $V_{\perp_B}$ = 10 m s^{-1}, V = V_z + 4 m s^{-1}. In the present case, since the drift is westward, V_z should be 4 m s^{-1} higher than the estimated velocity (i.e., V).

[38] In the presence of strong random fluctuations in the irregularity drift, the estimated V is expected to be higher than the true drift of the scintillation pattern because in this situation an assumed form of the space-time correlation function, first suggested by *Briggs* [1984], are not related to each other through the true drift V_0 of the moving pattern being studied but through $\sqrt{(V_0V_A)}$, where V_A is the so-called apparent drift which exceeds V_0. While the velocities estimated from the radar observations and those of scintillation broadly agree, there exists some difference as well. Given that the zonal drift (estimated from radar observations) is 30 m s^{-1} westward, which is primarily due to northward upward electric field, the zonal drifts estimated using scintillation observations, which are found to be higher than those of radar, appear to be partly due to the effect of zonal neutral wind.

4.3. On the Nature and Origin of the Irregularities

[39] Coming to the type of irregularities that were responsible for scintillation and U shape radar echoes, and also the underlying process, three specific observations that are of relevance are: (1) unusually large plasma density in the E_s patch, which was evident from the maximum f_tE_s (16 MHz), (2) scintillation observations indicating the presence of irregularity structures with spatial scale of 534 m (i.e., Fresnel dimension, d_F = 534 m), and (3) East-West asymmetry in spectral data for the two wings of the U shape structures. Especially the East-West SNR asymmetry (i.e., echo SNR is more in the right wing than those in the left wing) observed in the U shape structure is of practical relevance and reminds us about the well-known East-West power asymmetry linked with the electrojet E region plasma irregularities of the gradient drift instability origin. Such asymmetry has been explained by incorporating the tilted plasma density structures associated with the horizontally propagating primary gradient drift waves in the electrojet [*Patra et al.*, 2005b]. Considering that the spatial scale of the scintillation causing irregularities is 534 m, it can be assumed that structures with scale sizes in the range of 500–1000 km might have been present and acted as seed for the generation of secondary structures responsible for the radar observations and the observed asymmetry in SNR. These structures are very much expected from the theoretical expectation of kilometer-scale gradient drift wave structures during the daytime condition [*Ronchi et al.*, 1991]. However, if much larger-scale structures were present, for which we have no direct evidence, it is quite likely that neutral wind shear, that was possibly responsible for the formation of intense E_s, was also responsible for generating such structures through the Kelvin-Helmholtz (KH) instability. We also surmise that sharp density gradient associated with the unusually strong E_s played a significant role in generating the intense plasma density structures responsible for scintillation. Then the meter-scale irregularities responsible for radar observations then have been generated by the gradient drift instability process. Since the E_s layer formation at the lower E region requires vertical shear in zonal wind, having wind structure either westward wind above and eastward wind below or increasing value of westward wind with increasing height, it is quite expected that the E_s layer and associated irregularities would move westward by the westward neutral wind. Thus the westward drift observed in the present observations is consistent with this scenario.

[40] While the presumed primary plasma structures are quite consistent with those involved in the E region plasma turbulence and the scintillation observations, the sidelobe

detection of the irregularities, which is unusual, needs special properties. Considering that the intense daytime scintillation reported earlier were linked with strong blanketing type E_s activity [e.g., *Rastogi et al.*, 1977; *Rastogi and Mullen*, 1981], we surmise that the sidelobe detection of the plasma irregularities must be related to unusually large electron density structures linked with the intense E_s activity. The primary plasma structures then must be composed of unusually large peak density with tilted phase fronts akin to the electrojet primary gradient drift waves reported earlier. These primary waves are known to provide conditions for the secondary plasma waves to grow in preferential direction [*Patra et al.*, 2005b] manifesting secondary plasma irregularities with adequate density gradients to be detected by the sidelobes. We surmise that the key issues were the plasma structures with unusually large localized density and their preferential orientation, which were possibly generated by the gradient drift process on the vertical density gradient of the unusually intense E_s patch or by KH instability [*Hysell et al.*, 2002a].

[41] Having discussed that intense plasma density structures embedded in strong E_s layers were responsible for scintillation and mysterious radar echoes, we would like to bring in other implications of intense E_s plasma cloud. One aspect is the high altitude daytime radar echoes from the *E* region reported by *Yokoyama et al.* [2009]. We believe that they were also possibly due to the sidelobe detection of the *E* region echoes of plasma cloud origin. The large range of the echoes and associated East-West power asymmetry reported by *Yokoyama et al.* [2009] fit quite well with the premise proposed to account for the mysterious high-altitude radar echoes reported here. Their case did not reveal so many high-altitude clumps, possibly due to low transmitted power involved in the EAR system used by them. This implies that the *E* region plasma irregularities of intense plasma cloud origin could be very different and would be detected by the sidelobes of radars with even well-designed antenna array, such as those of the Gadanki radar and the EAR. Interpretation of such observations without knowing the angle-of-arrival of the echoes would be quite misleading and such observations demand suitable interferometric observations to obtain the angle-of-arrival of the echoes. This implies that radar echoes arising out of intense E_s plasma cloud could be difficult to interpret without having interferometry. Plasma cloud could also refract radio wave significantly (up to about 2°) [*Hysell et al.*, 2002b] facilitating radar observations of plasma irregularities better in some direction than in other direction, which can manifest as East-West power asymmetry. Another aspect is linked with the effect on GPS radio occultation (RO) signals discussed by *Zeng and Sokolovskiy* [2010]. It has been shown that when the E_s plasma clouds are aligned with the propagation direction, they could cause defocusing and scintillation of the GPS RO signal which are being received by the low-Earth orbiting satellite. This implies that plasma cloud of the type reported here could be detrimental for GPS RO based atmospheric measurements.

5. Conclusions

[42] We have analyzed a unique observational data set of unusually high-altitude *E* region radar echoes and VHF scintillation linked with a daytime strong E_s patch observed from Gadanki, not encountered before. We have shown that the unusually high-altitude radar echoes are due to the sidelobe detection of plasma irregularities of special type that were generated on the intense E_s patch. The primary plasma structures, which caused intense daytime scintillation at 250.6 MHz, are possibly generated by kilometer-scale gradient drift instability process or KH instability by the neutral wind on the sharp density gradients associated with the intense E_s patch. Importantly, these structures seem to be consisting of large density and density gradients and have tilted phase fronts so that they will easily be unstable generating secondary plasma structures with strong angular anisotropy. The implications of such primary plasma structures is that they could give rise to special structures that would provide condition for the sidelobe detection of radar echoes manifesting high-altitude radar echoes as artifacts and also for defocusing/scintillation of GPS RO signal.

[43] **Acknowledgments.** Authors gratefully acknowledge NARL technical staff for making the observations reported here.

[44] Robert Lysak thanks the reviewers for their assistance in evaluating this paper.

References

Bhattacharyya, A., and R. G. Rastogi (1986), Multifrequency spectra of day-time ionospheric amplitude scintillations near the dip equator, *J. Atmos. Terr. Phys.*, *48*, 463–469, doi:10.1016/0021-9169(86)90123-6.

Briggs, B. H. (1984), The analysis of spaced sensor records by correlation techniques, in *Middle Atmosphere Program: Handbook for MAP*, vol. 13, edited by R. A. Vincent, pp. 166–186, SCOSTEP, Boulder, Colo.

Chau, J. L., R. F. Woodman, and L. A. Flores (2002), Statistical characteristics of low latitude ionospheric field-aligned irregularities obtained with Piura VHF radar, *Ann. Geophys.*, *20*, 1203–1212, doi:10.5194/angeo-20-1203-2002.

Choudhary, R. K., J.-P. St.-Maurice, L. M. Kagan, and K. K. Mahajan (2005), Quasi-periodic backscatters from the *E* region at Gadanki: Evidence for Kelvin-Helmholtz billows in the lower thermosphere?, *J. Geophys. Res.*, *110*, A08303, doi:10.1029/2004JA010987.

Hysell, D. L., M. Yamamoto, and S. Fukao (2002a), Simulation of plasma clouds in the midlatitude E region ionosphere with implications for type I and type II quasiperiodic echoes, *J. Geophys. Res.*, *107*(A10), 1313, doi:10.1029/2002JA009291.

Hysell, D. L., M. Yamamoto, and S. Fukao (2002b), Imaging radar observations and theory of type I and type II quasi-periodic echoes, *J. Geophys. Res.*, *107*(A11), 1360, doi:10.1029/2002JA009292.

Krishna Murthy, B. V., S. Ravindran, K. S. Viswanathan, K. S. V. Subbarao, A. K. Patra, and P. B. Rao (1998), Small-scale (∼3 m) *E* region irregularities at and off the magnetic equator, *J. Geophys. Res.*, *103*, 20,761–20,773, doi:10.1029/98JA00928.

Li, Z., L. Liu, W. Wan, and B. Ning (2011), Neutral wind-driven gradient drift instability in the low-latitude daytime *E* region, *J. Geophys. Res.*, *116*, A03314, doi:10.1029/2010JA016166.

Patra, A. K., and N. V. Rao (2006), Radar observations of daytime 150-km echoes from outside the equatorial electrojet belt over Gadanki, *Geophys. Res. Lett.*, *33*, L03104, doi:10.1029/2005GL024564.

Patra, A. K., and N. V. Rao (2007), Further investigations on 150-km echoing riddle using simultaneous observations of 150-km and *E* region echoes from off-electrojet location Gadanki, *J. Geophys. Res.*, *112*, A09301, doi:10.1029/2006JA012204.

Patra, A. K., S. Sripathi, V. Sivakumar, and P. B. Rao (2004), Statistical characteristics of VHF radar observations of low latitude *E* region field-aligned irregularities over Gadanki, *J. Atmos. Sol. Terr. Phys.*, *66*, 1615–1626, doi:10.1016/j.jastp.2004.07.032.

Patra, A. K., S. Sripathi, P. B. Rao, and K. S. V. Subbarao (2005a), Simultaneous VHF radar backscatter and ionosonde observations of low-latitude *E* region, *Ann. Geophys.*, *23*, 773–779, doi:10.5194/angeo-23-773-2005.

Patra, A. K., D. Tiwari, C. V. Devasia, T. K. Pant, and R. Sridharan (2005b), East-west asymmetries of the equatorial electrojet 8.3 m type-2 echoes observed over Trivandrum and a possible explanation, *J. Geophys. Res.*, *110*, A11305, doi:10.1029/2005JA011124.

Patra, A. K., T. Yokoyama, M. Yamamoto, T. Nakamura, T. Tsuda, and S. Fukao (2007), Lower *E* region field-aligned irregularities studied using the Equatorial Atmosphere Radar and meteor radar in Indonesia, *J. Geophys. Res.*, *112*, A01301, doi:10.1029/2006JA011825.

Patra, A. K., N. Venkateswara Rao, D. V. Phanikumar, H. Chandra, U. Das, H. S. S. Sinha, T. K. Pant, and S. Sripathi (2009), A study on the low-latitude daytime *E* region plasma irregularities using coordinated VHF radar, rocket-borne, and ionosonde observations, *J. Geophys. Res.*, *114*, A11301, doi:10.1029/2009JA014501.

Rao, P. B., A. R. Jain, P. Kishore, P. Balamuralidhar, S. H. Damle, and G. Viswanathan (1995), Indian MST radar, 1. System description and sample wind measurements in ST mode, *Radio Sci.*, *30*, 1125–1138, doi:10.1029/95RS00787.

Rastogi, R. G., and J. Mullen (1981), Intense radio wave scintillation and sporadic *E* layer near the dip equator, *J. Geophys. Res.*, *86*, 195–198, doi:10.1029/JA086iA01p00195.

Rastogi, R. G., M. R. Deshpande, B. S. Murthy, and K. Davies (1977), Daytime satellite radio scintillation and sporadic *E* near the magnetic equator, *Geophys. Res. Lett.*, *4*, 113–115, doi:10.1029/GL004i003p00113.

Ronchi, C., R. N. Sudan, and D. T. Farley (1991), Numerical simulations of large-scale plasma turbulence in the daytime equatorial electrojet, *J. Geophys. Res.*, *96*, 21,263–21,279, doi:10.1029/91JA01951.

Rufenach, C. L. (1972), Power-law wavenumber spectrum deduced from ionospheric scintillation observations, *J. Geophys. Res.*, *77*, 4761–4772, doi:10.1029/JA077i025p04761.

Sudan, R. N. (1983), Unified theory of type 1 and type 2 irregularities in the equatorial electrojet, *J. Geophys. Res.*, *88*, 4853–4860, doi:10.1029/JA088iA06p04853.

Venkateswara Rao, N., A. K. Patra, and S. V. B. Rao (2008), Some new aspects of low-latitude *E*-region QP echoes revealed by Gadanki radar: Are they due to Kelvin-Helmholtz instability or gravity waves?, *J. Geophys. Res.*, *113*, A03309, doi:10.1029/2007JA012574.

Yokoyama, T., D. L. Hysell, A. K. Patra, Y. Otsuka, and M. Yamamoto (2009), Zonal asymmetry of daytime 150-km echoes observed by Equatorial Atmosphere Radar in Indonesia, *Ann. Geophys.*, *27*, 967–974, doi:10.5194/angeo-27-967-2009.

Zeng, Z., and S. Sokolovskiy (2010), Effects of sporadic *E* clouds on GPS radio occultation signals, *Geophys. Res. Lett.*, *37*, L18817, doi:10.1029/2010GL044561.

A. Bhattacharyya, Indian Institute of Geomagnetism, Plot No. 5, Sector 18, Navi Mumbai, Maharashtra 410218, India.

P. P. Chaitanya, Department of Physics, Sri Venkateswara University, Tirupati, 517502 India.

A. K. Patra, National Atmospheric Research Laboratory, Gadanki, Chitoor, Andhra Pradesh 517112, India. (akpatra@narl.gov.in)